Illumination of Gold Nanoparticles for Tumor Angiogenesis

Ishwer Mahore[1], G. F. Ansari[2], Savita Tiwari[3]

[1](Faculty of Science and IT, Madhyanchal Professional University, Bhopal, India)
[2, 3](Faculty of Science and IT, Madhyanchal Professional University, Bhopal, India)
[1]Corresponding Author: researchindia05@gmail.com

Abstract: *This paper reports on the evolution of tumor-specific gold nanoparticles (AuNPs) as theranostic tools intended for target accumulation and the detection of tumor angiogenesis via ocular image (OI) before diagnosis is started, before initiation with an external X-ray radiation source. The AuNPs were decorated with a near-infrared dye, and RGD peptides as the tumor targeting vector for αvβ3-integrin, which is overexpressed in tissue with high tumor angiogenesis. The AuNPs were examined in an ocular image setting in vitro and in vivo exhibiting approving diagnostic properties with regards to tumor cell accumulation, bio-distribution, and clearance. Further- more, the therapeutic features of the AuNPs were evaluated in vitro on pUC19 DNA and on A431 cells concerning acute and long-term toxicity, indicating that these AuNPs could be useful as radio-sensitizers in therapeutic concepts in the future.*

Keywords: *Nanoparticle, Occular Imaging, Radio-sensitive, Angiogenesis; Peptides, Illumination, Fluorescence*

_____

I.   Introduction

In recent years, gold nanoparticles (AuNPs) have gained serious attention since their first use as radioactive Au-nano-colloid in theearly 1950s for nano-brachytherapy. Since then, the focus has shifted to the manufacturing of ultra-small target-specific AuNPs with a very narrow size distribution and, ultimately, tailored shapes for used in various imaging modalities such as CT, Raman, or photoacoustic imaging. On the one hand AuNPs represent a perfect platform for multimerization of target-specific effectors on their surface and on the other hand they offer the possibility of detection using multi- modal imaging techniques by surface modification, as well as for therapeutic purposes. Many approaches of AuNPs with a size of >10 nm are elicited from a phenomenon known as 'enhanced permeability and retention' (EPR) effect due to passive extravasation of nanoparticles over the perforated vasculature of tumors. Rapid renal clearance is preferred for radioactive discriminating nanoparticles to bypass a high radiation on healthy tissues, which can be accomplished for AuNPs smaller than 6nm in diameter.

The evaluation of methods for the synthesis of ultra-small (<5 nm) AuNPs followed by surface-modification for enhanced stability and homogenization paved the way for functionalization. The high attraction of sulfur for gold surfaces and the pattern of stable and covalent Au-S bonds enable a fast and facile functionalization of AuNPs with thiol-modified (bio)molecules. Furthermore, PEGylation of the AuNPs leads to a higher bioavailability, as it hinders in vivo formation of a protein corona around the AuNPs. Therefore, ultra-small target-specific AuNPs can be developed and functionalized with small molecules, antibodies, peptides, and natural products. For molecular imaging, AuNPscan be functionaries with near-infrared dyes, with radionuclides like fluorine-18, copper-64 or gallium- 68 for PET, and with Magnetic Resonance Imaging (MRI)-relevant metals like gadolinium.

Additionally, their therapeutic application, and particularly theability to be applicable as a radio-sensitizer by Auger- Meitner electron (AME) emission induced by external gamma activation or β- emission of 412 keV electrons induced by neutron activation of natural 197Au generating [198Au]AuNPs are of special interest. The focus of this work is depend on the development of theragnostic agents using targeted gold nanoparticles for near-infrared (NIR) fluorescent optical imaging (OI). Sur- face-functionalization was easily achieved by ligand exchange, introducing, in other hand different reporter or targeting moieties, functional groups for further chemo-selective

_____

conjugation to which complementary functionalized targeting vectors are then attached. The RGD peptides motif is known to bind to the trans-membrane αvβ3 integrin thatoverexpressed during tumor angiogenesis for example on glioma (U87MG) or on epidermis (A431) cells. To achieve target-specific accumulation in tissue with high tu- mor angiogenesis, the AuNPs were functionaries with a c(RGDfK) derivative.

II. Material And Methods

All reagents and solvents were purchased from commercial sup- pliers and were used without further purification. NIR-dye (SIDAG precursor) was purchased from Chess, Mannheim, Germany. NMR spectra were recorded on a 300 MHz Varian Mercury Plus or a 500 MHz Varian NMR System spectrometer (Palo Alto, CA, USA). Chemical shifts (δ) are given in ppm and are relative to (CH3)4Si (1H, 13C). Mass spectra obtained on a BrukerDaltonicsmicro flex MALDI-TOF mass spectrometer (Bremen, Germany). The Preparative column chromatographies areperformed on Merck silica gel G60. Changes was monitored by thin-layer chromatography (TLC) on Merck silica gel F254 aluminum plates, with observe under UV (λ = 254 nm) or by evaluation using ninhydrin and heating. If necessary, the purity was determined by high performance liquid chromatography (HPLC). The purity of all final compounds was 95% or higher. HPLC was performed on a DionexUltiMate 3000 HPLC system (Thermo Scientific, Dreieich, Germany), equipped with a reverse phase column (Analytical: Merck Chromolith RP-18e; 100×4.6 mm plus a guard column 5×4.6 mm; semi preparative: Chromolith RP-18e; 100×10 mm plus a guard column 10×4.6 mm), and a UV-diode array detector (210 nm, 254 nm).

The solvent system used was a gradient of acetonitrile:water (containing 0.1% TFA) (0–5 min: 0–100% MeCN) at a flow rate of 4 mL/min unless otherwise stated. The purification of AuNPs was performed via dialysis (molecular weight cut-off of 14,000 g/mol, Visking, Roth) against distilled water and via size-exclusion chromatography using Se- phadex G25 PD10 columns and distilled water as eluent. The purity of the AuNPs was verified by size exclusion HPLC using a PhenomenexPolySep™-SEC GFC-P 4000, LC Column 300×7.8 mm and a 35 mm PolySep guard column with water (0.8 mL/min) as eluent on a ThermofisherUlti HPLC system. Irradiation experiments were performed in an X-ray chamber on a Maxishot Y.TU 320-D03 (Yxlon, Hamburg, Germany) (200 kV, 20 mA, dose rate D = 1.24 Gy/min). Re-188-solution was obtained by elution with 0.9% NaCl from an 188W/188Re-generator (OncoBeta, Garching, Germany). The eluat was concentrated by a QMA cartridge (WAT023525, Waters, Eschborn, Germany), and eventually eluted W- 188 was trapped on an alumina cartridge (WAT023561, Waters).

Thiol-PEG3-OH and furan-protected thiol-PEG4-maleimide [50] were synthesized ac- cording to Zhu et al. without any modification. A brief description of the AuNPsyn- theses can be found in the supporting information.

The αvβ3-binding affinities of the RGD peptides and the respectively modified AuNPs were determined on A431 tumor cells by in vitro competitive displacement experiments. A431 cells was seeded onto 24-well plates 2–3 days prior to assay start to reach 0.4–0.5×106 cells per well. A special binding buffer (Tris·HCl 25 mM, NaCl 150 mM, CaCl2 1 mM, MgCl2 0.5 mM, MnCl2 1 mM, pH 7.4, BSA 0.5%) were used for incubation with 0.13 nM 125I-Echistatin (81.4 GBq/µmol) as the αvβ3-specific radiolig in the presence of high concentrations (0–100 µM) of competing c(RGDfK) pep- tide or c(RGDfK)-modified AuNPs (0–30 µM). The IC50 value wasgenerated using the software Origin v9.6.0.172 (Nonlinear Fit, Growth/Sigmoidal, Dose Resp, Levenberg Mar- quardt Fit).

Fluorescence microscopy on Leica TCS SP8. For fluorescence microscopy, cells were seeded onto coverslips for more than 2 days, then wash with PBS and incubated for 1, 3, 6, and 24 h at 37 °C in 5% CO2 with the respective media containing AuNPs (100 µg/mL, 0.33 µM). For blocking experiments, c(RGDfK) (150 µg/mL, 0.25 mM) were added to the wells together with AuNPs. Afterwards, the cells are washed with PBS and incubated with CellMask Orange-solution (1 × working solution) for 15 min at 37 °C. Cells were fixed with 1:1 medium: 4% formaldehyde in PBS for 2 min at ambient temperature and then with 4% formaldehyde in PBS for 15 min at ambient temperature.Cells are then wash 3 × with PBS, coverslips were prepared onto an object plate with Sytox Green-solution (8.3 µM, 10 µL). Fluorescence microscopy was performed on a Leica TCS SP8 confocal microscope with lasers at λ = 488, 552 and 638 nm. An overlay of microscopies was generated using the FIJI software (v1.50e).

Three days prior to the experiments, 150,000 cells were seeded into a 6-well plate. A431 cells are incubated for 24 h in the presence or the absence of the αvβ3-specific or non-specific AuNPs. After incubation in the presence or the absence of the AuNPs, the cellsare washed, and the cell medium was refreshed. Subsequently, the cells were irradiated with X-rays (Maxishot Y.TU, Yxlon, Hamburg) up to 12 min to reach a maximum dose of 10 Gy. After irradiation, the cells are harvested, a colony formation assay was performed in triplicate for each irradiation point with 1000 cells per well in a 6-well plate. Colonies were cultivated in cell medium for 7 days and then washed with 1 mL PBS, fixed with 2 mL 80% ethanol for 10 min and incubated with 2 mL crystal violet dye solution for 30 min. Afterwards, colonies were washed with distilled water, dried, and counted by light microscopy. Colonies of more

than 50 cells were deemed to be survivors, and the plating efficiency for each sample was estimated based on the initial number of seeded cells. The clonogenic cell survival was calculated as the relative plating efficiency of treated vs. untreated samples. Triplicate samples were prepared for each treatment and experimental condition.

The in vivo proof-of-concept was performed using male athymic nude mice (Rj:ATHYM-Foxn1nu/nu) obtained from Janvier Labs. 5×106 A431 cells (100 μL, PBS with or without matrigel:PBS v:v = 1:1, unsieved) were inoculated subcuta- neously in the left thigh when the mice was 57 weeks old. Mouse health and tumor growth were checked daily until the tumor reached a diameter of 2–5 mm (3–6 weeks for A431). Tumor growth was slower for the matrigel injection and the tumor was smaller. After the tumors reached a sufficient size for imaging, the AuNPs were injected intravenously into the tail vein and their distribution in vivo was monitored after 1, 2, 4, 24, 28, 48, and 72 h via optical imaging (excitation 730 nm, emission 790 nm, 60 s) followed by X- ray imaging (0.8 mm filter, 45 kV, 5 s) (In Vivo Xtreme, Bruker, Ettlingen). After the last time point, animal are sacrificed, the organs were harvested, and measured ex vivo with the In Vivo Xtreme system. The region of interest (ROI) was drawn by hand on the organs for calculation of the uptake of the AuNPs in the respective organs. Amide (v1.0.4) was used for the fusion of the images. All injection and measurements with mice are performed by anesthesia (2–3% isoflurane/O2, 2–3 mL/min).

III. Result

Synthesis and Functionalization of Gold Nanoparticles

Integrin αvβ3, a trans-membrane protein expressed on endothelial cells, and binds the Arg-Gly-Asp (RGD) triple peptide motif of extracellular matrix proteins. Growing malignant tumors continuously requires angiogenesis, and for this purpose the integrin αvβ3 is overexpressed. As a result, αvβ3 is preferentially expressed in tumor angiogenesis and is a potential target for AuNPs decorated with RGD peptides. Therefore, ultra-small AuNPs (3 ± 2 nm) were synthesized by the Brust-Schiffrin-method with thiol-PEG3- OH used as the stabilizing ligand and to achieve an increased biocompatibility. The AuNPs were further functionalized via ligand exchange with furan-protected maleimide- PEG4-thiol (Figure 1). Afterwards, the furan-maleimide-AuNPs 2a were deprotected at 95°C in DMSO for 2 h (2b), followed by the attachement with the thiol-functionalized αvβ3- specific ligand thiol-c(RGDfK) 6 (Figure 1) and the thiol-functionalized fluorescent dye 3 (Figure 1).
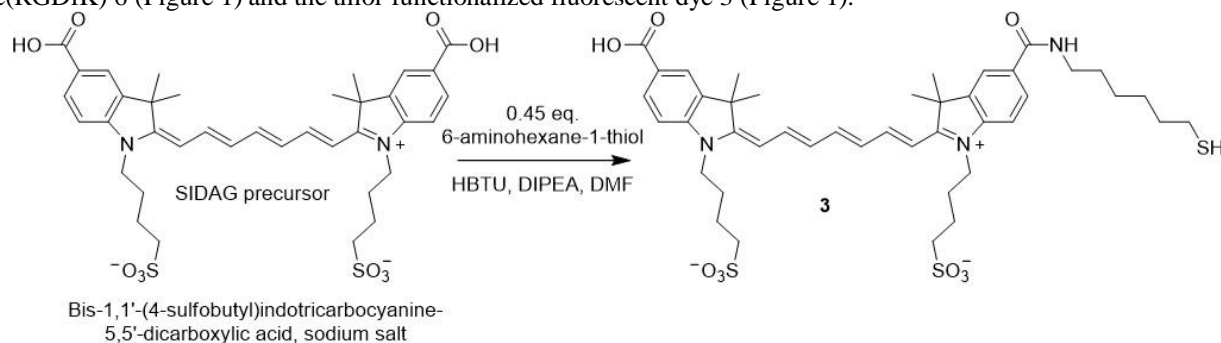

Figure no 1: Cyanine derivative (SIDAG precursor [49]) and thiol-functionalized derivative 3 for coupling reactions via Michael addition

For the use in OI, the AuNPs were functionalized with 3, which was performed at a ratio of 40:1 (AuNPs:dye).

Using more NIR-dye resulted in the aggregation of the AuNPs as well as decreased fluorescence signals due to self-quenching. The purification of the AuNPs was performed via dialysis and size-exclusion chromatography. The AuNPs 7 and 8 were incubated with PBS, rat plasma, and cell media for at least 24 h at 37°C, and no aggregation was found. Their stability was finalizeby UV/Vis spectroscopy and HPLC. The AuNP-RGD-NIR-dye 8 exhibited very low photobleaching (<3% within 24 10h at 37 °C) and enabled biocompatible fluorescence in the optical window of tissue, with absorption of 600–800 nm (AbsMax = 750 nm) and emission at 750–820 nm (EmMax = 780 nm).

The loss of mass of the AuNPs was identified by thermo-gravimetric analyses for each functionalization step. The measurements were compared between the product and educts to identify the additional loading of the respective functionalization step. There- fore, the difference in the loss of mass of product and educt gave the total mass of newly attached molecules. The mean number of newly attached molecules could be estimated by dividing the mass difference by the molar mass of the respective molecule. After know- ing the numbers of the newly attached molecules, a formula from Zhu et al. was use to calculate the total molar mass of the AuNPs (Table 1).

A brief detail of the synthesis and characterization can be found in the appendix. All AuNPs were fully characterized by thermo-gravimetric analysis (TGA) (Figures 3–4), UV/Vis spectroscopy (Figures 5–6), electron microscopy (EM) (Figure 7 and 8), HPLC (Table 1), dynamic light scattering (DLS) (Table 2), and NMR (Figure 9– 10). The dynamic light scattering was performed on a Malvern Zetasizer ZS90. AuNPs were dissolved in distilled H2O at a concentration of 1 μg/mL. All values are the mean value of at least three different measurements. If the poly-dispersity index (PDI) is >0.5 the size by number is more relevant than the size by volume. The size by number is best comparable to the size measured by EM. The AuNPs could be stored in lyophilized form for >12 months at −20 °C without losing their integrity. In contrast, if stored in solution at room temperature, aggregation in form of precipitation occurred within weeks, especially for peptide- or NIR-decorated particles.
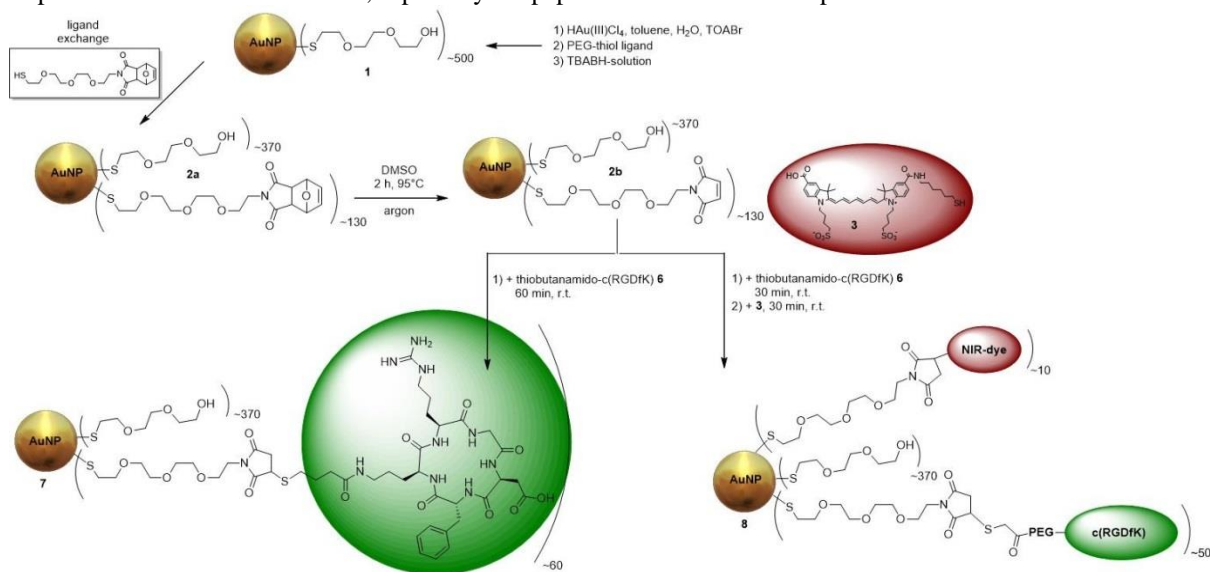

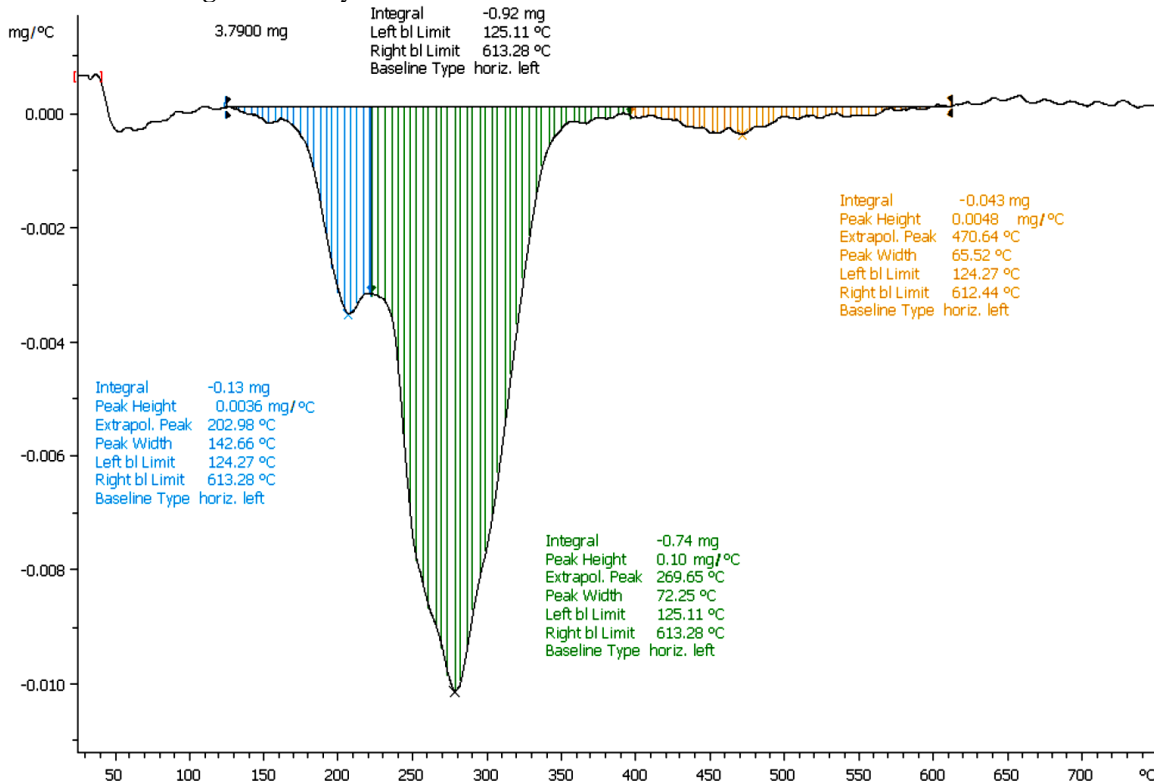**Figure no 2:** Synthesis of the different RGD-functionalized AuNPs 7 and 8

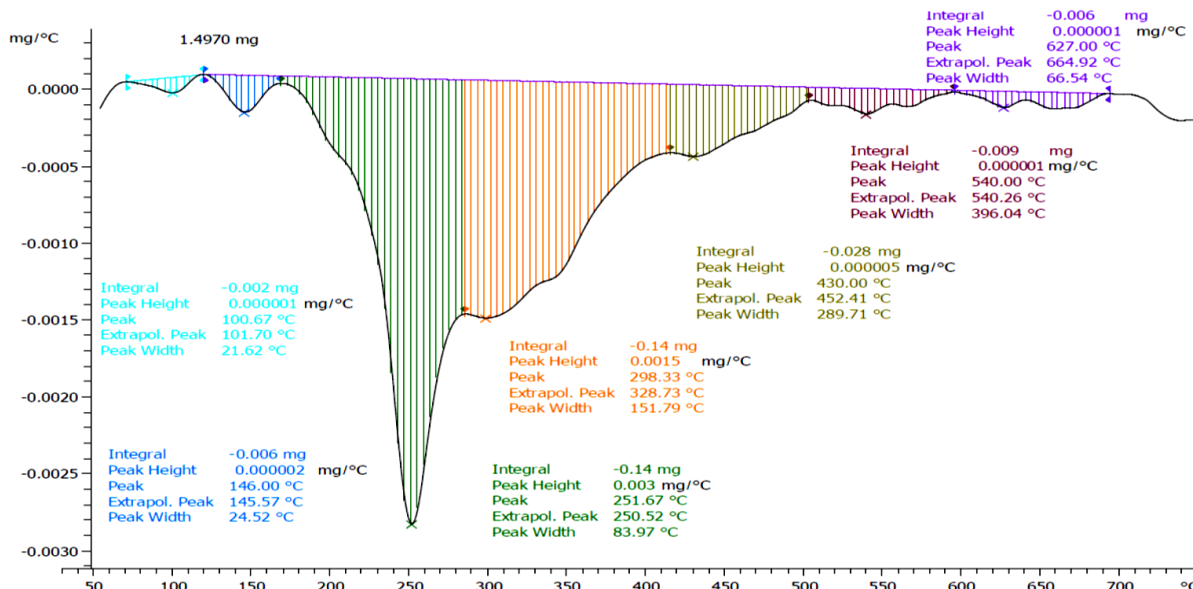**Figure no 3:** AuNP-PEG 1 with mass loss of ~24.27%

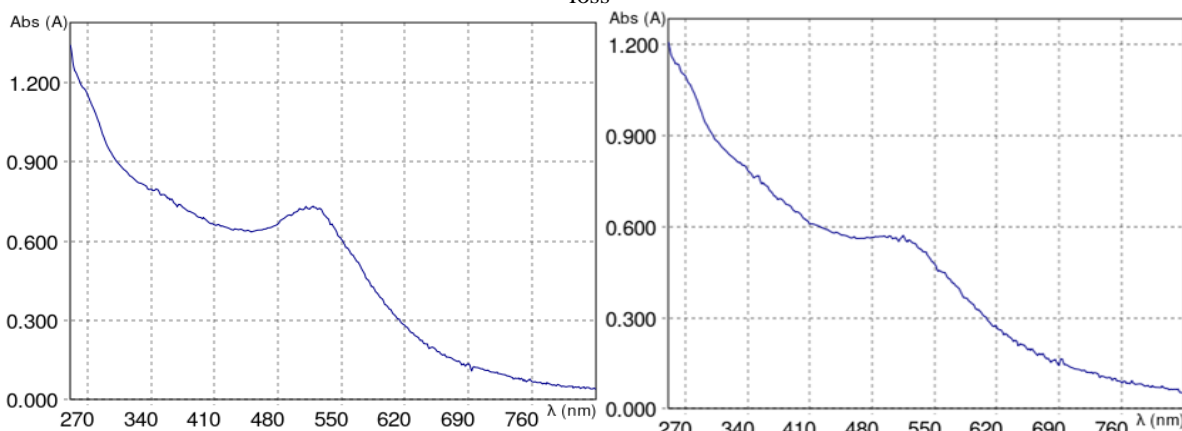**Figure no 4:** AuNP-RGD-NIR-dye 8 with mass loss of ~22.17%. The NIR-dye-ligands accounts for 0.46% mass loss

Figure no 5: AuNP-PEG 1 (Aspr = 0.730/A450 = 0.633 give 1.15 → 3–4 nm) after dialysis with typical absorption maximum for ultrasmallAuNPs at 514 nm (left). AuNP-maleimide2a (right)
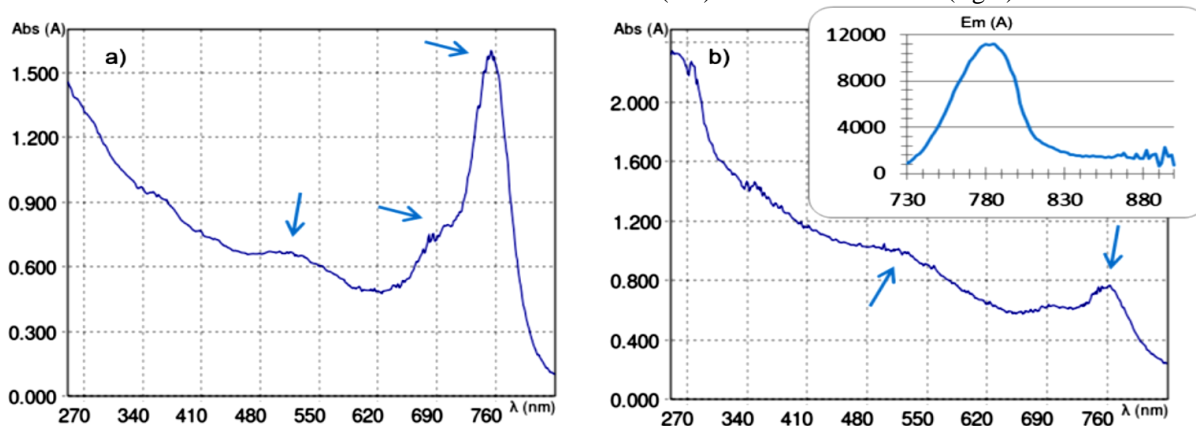

Figure no 6: Absorption spectra of AuNP-RGD-NIR-dye 8 (a) after dialysis and (b) after additional Sephadex purification (Aspr = 0.668/A480 = 0.660 gives 1.01 → 3 nm) with three absorption maxima at 534, 690, and 750 nm. Insert in (b): Corresponding emission spectrum (excitation wavelength = 690 nm, emission = 740–840 nm, EmMax = 790 nm)

Table no 1: Calculated number of ligands and resulting molecular mass of the AuNPs and retention in HPLC

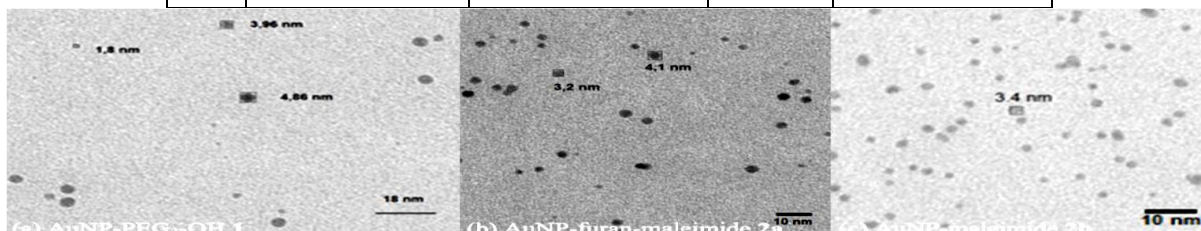| Probe	Description	Number of Ligands	Molecular Mass [kDa]	Retention Time HPLC [min]
1	AuNP-PEG	500 PEG3-OH	345	6.48
2a	AuNP-PEG-maleimide	130 PEG4-maleimide	361	6.10
7	AuNP-RGD	60 RGD	405	5.98
8	AuNP-RGD-NIR-dye	~50 RGD, 10 NIR-dye	413	6.20

Figure no 7: Transmission electron microscopy of (a) AuNP-PEG 1 (A = 10.53 nm2, Ø = 3.66 nm, n =1000), (b) AuNPs 2a, and (c) AuNPs 2b (A = 9.21 nm2, Ø = 3.42 nm, n = 1860)
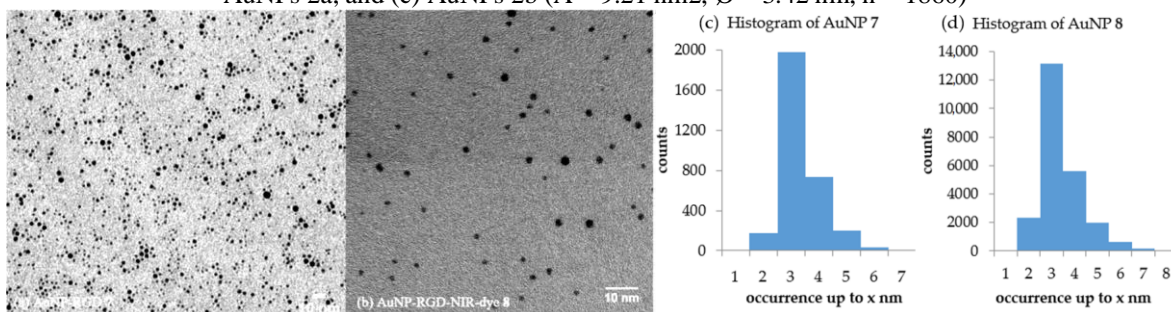

Figure no 8: Transmission electron microscopy of (a) AuNP-RGD 7 (A = 6.64 nm2, Ø = (2.91 ± 2.27) nm, n = 3100) and (b) AuNP-RGD-NIR-dye 8 (A = 7.44 nm2, Ø = (3.08 ± 2.57) nm, n = 23,900) and the respective histograms (c) and (d) of the AuNP diameter distribution

Table no 2: Different expressions of the hydrodynamic radius of the AuNPs measured by DLS

Probe	Size by Number [nm]	Size by Volume [nm]	Z-Averge [nm]	PDI
1	7.2	8.7	311	0.555
2a	14.1	13.6	209	0.456
7	33.8	32.6	713	0.883
8	53.8	59.8	174	0.403

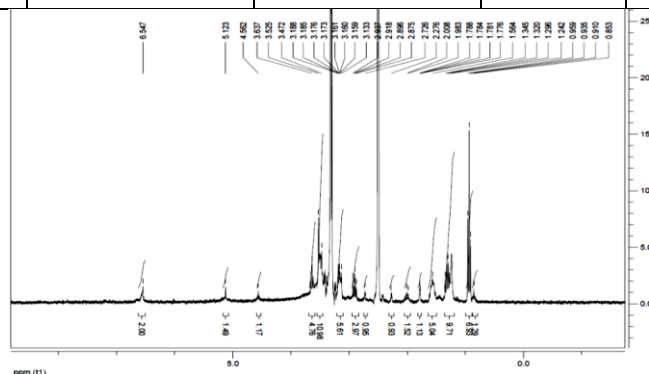**Figure no 9:** 1H NMR spectrum of AuNPs 2a in d6-DMSO with the characteristic signals of the furan protected maleimide at 6.55, 5.12, and 4.56 ppm
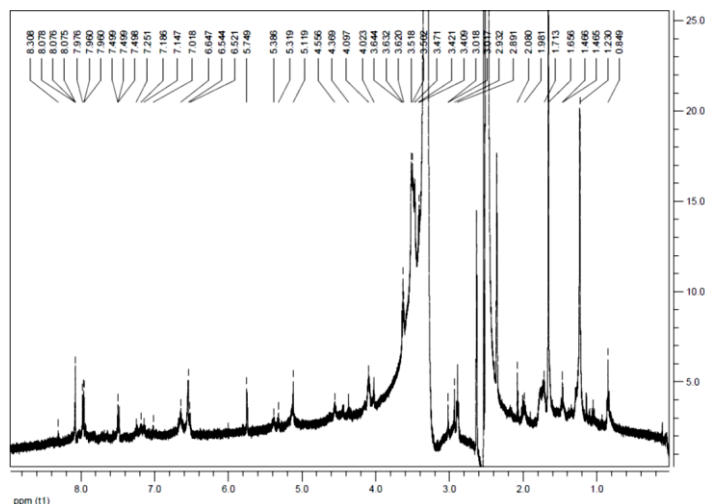
Figure no 10: 1H NMR spectrum of AuNP-RGD-NIR-dye 8 in d6-DMSO: typical signals of peptidebond-NH (7.50 ppm), Phe-CHarom (7.25–7.02 ppm), Arg-C=NH (6.65 ppm), Arg-NH2 (5.75 ppm), Phe-CH (5.39 ppm), Asp-CH (5.32 ppm), Arg-CH (4.56 ppm), Lys-CH (4.37 ppm), Gly-CH2 (4.02 ppm) and NIR-dye 8.08 (d, 2H, 6,6′-H), 8.05 (s, 2H, 4,4′-H), 7.96 (t, 2H, β,β'-H), 7.50 (m, 1H, δ-H), 7.3 (d, 2H, 7,7′-H), 6.65 (t, 2H, γ,γ'-H), 6.54 (d, 2H, α,α'-H), 4.09 (t, 4H, 2 × >NCH2) (compound 4a in [51]) can be found

Cell Experiments

Several different IC50 values for RGD derivatives are already available in literature, ranging from 0.1 nM up to 6.7 µM. The mainreason for the observed differences is the assay method used to determine the IC50 values. IC50 values of 0.1–1 nM can be found for RGD peptides having been determined by ELISA assays and IC50 values around 20 nM were reported for solid-phase αvβ3 binding assays for monomeric RGD derivatives. Those IC50 values were derived by non-living experiments. Cell experiments are closer to in vivo condition. Therefore, for the AuNPs 7 and 8, the αvβ3-avidities were determined by competitive displacement experiments on αvβ3-expressing A431 cells using 125I-Echistatin as αvβ3-specific radioligand and competitor (Figure 11). As internal reference, the RGD monomer c(RGDfK) was evaluated.

With the evaluation of RGD derivatives by displacement experiments, IC50 values comparable with those in existing literature were found. For c(RGDfK) a IC50 value of (1.75 ± 0.84) µM was found. The multi- RGD decoration at the surface of AuNP 7 led to a lower IC50 value of (1.07 ± 0.74) µM compared to the isolated RGD monomer. Further function of the AuNPs with cyanine dye 3 led to a slightly higher IC50 value of (3.37 ± 0.73) µM for AuNP 8.

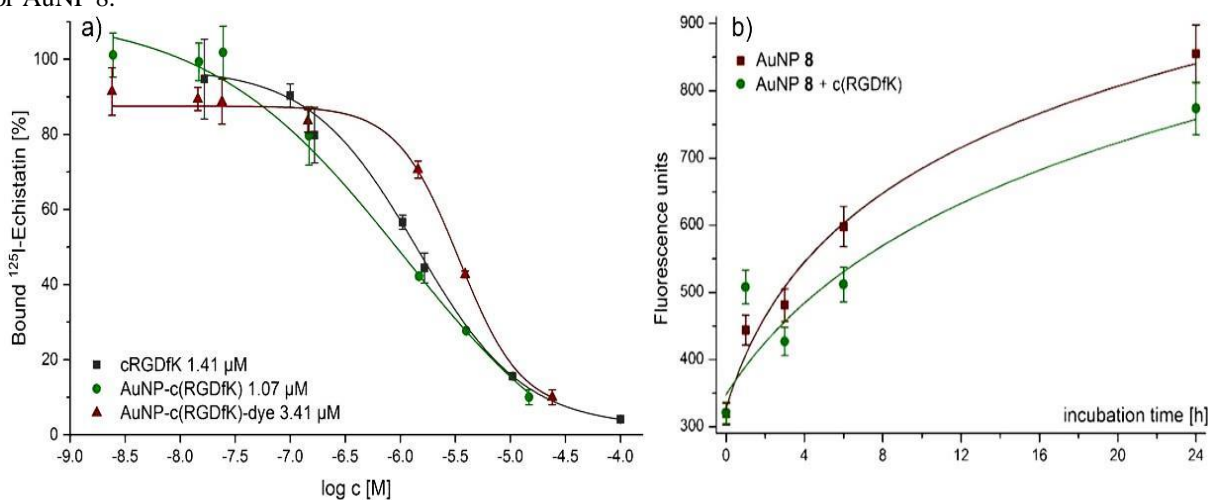**Figure no 11:** (a) Three representative IC50-curves from single competitive binding experiments. Shown is one curve with single IC50 value out of three values from three different experiments.
(b) Cell uptake studies of AuNPs 8 in A431 cells at different time points obtained without blocking (red) andwitha10-fold excess of c(RGDfK)(green)

Next, the cellular uptake of AuNPs 8 was evaluated on A431 cells at different time-points from 1–24 h. An at least partly receptor-specific uptake was found for the AuNPs (Figure 12b), as the cellular uptake of the dually modified particles could be partly blocked by pre-incubation using a 10-fold excess of c(RGDfK) 1 h before incubation with AuNPs. Furthermore, the AuNPs 8 were tested for their behavior in vitro on A431 cells via fluorescence microscopy. First, the concentration for optimal microscopy was evaluated in a concentration range between 10–100 µmol/mL after an incubation time of 24 h. These initial cell studies revealed an optimized concentration of 50 µg/mL of AuNPs 8 for cell imaging. Next, via confocal fluorescence microscopy, the cell internalization, and the fate of the AuNPs were observed at different time points from 1–24 h (Figure 12).
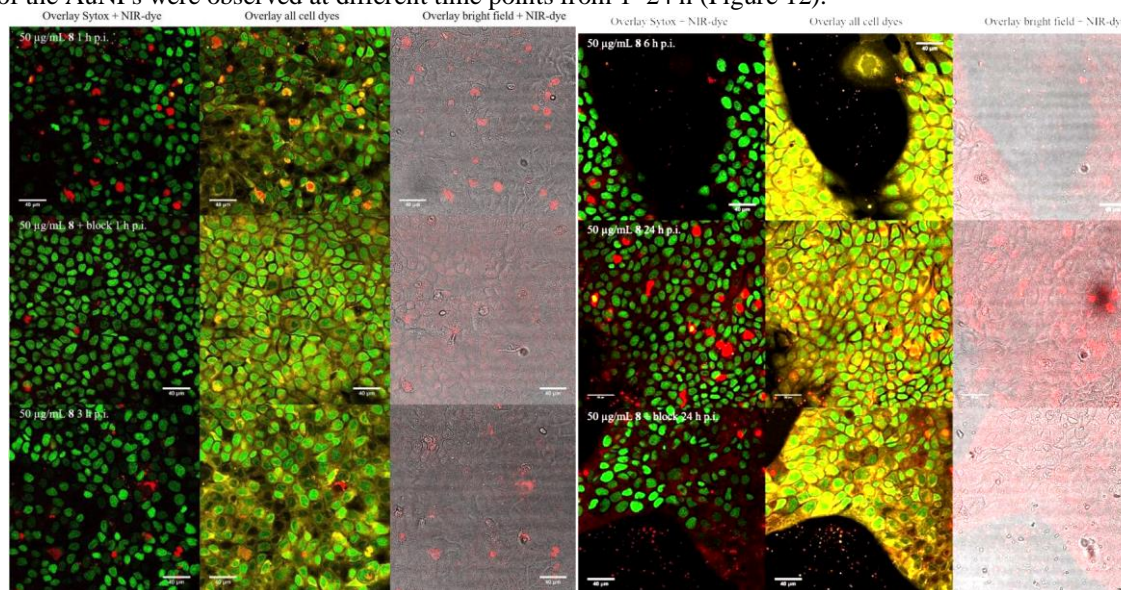

Figure no 12: Fluorescence microscopy of A431-cells incubated with AuNP-RGD-NIR-dye 8 at same concentrations (50 µg/mL) at 1, 3, 6, and 24 h (from top to bottom). Left row overlays of Sytox Green and 8 are shown. Middle row overlays of Sytox, membrane orange and 8 are shown. Right row overlays of bright field and 8 are shown. The cell nuclei were stained with Sytox Green and the cytoplasma with membrane Orange

The con- focal microscopy images revealed several findings: The number of observed fluorescence foci in the cells rises within the observation time from 1–24 h indicating an accumulation of AuNPs within the cell plasma. Further, these foci become bigger after 1 h of incubation. The AuNPs accumulated most probably in vesicles within the cells. At later time-points, the vesicles appeared to become smaller containing less particles, whereas several new and much smaller foci showed up outside the cells. This is perhaps explained by the formation (and their later excretion) of vesicles containing the AuNPs. The conclusion that the mentioned dots represent vesicles is confirmed by the fact that structures can be stained with membrane Orange, but not with the nuclei marker Sytox Green. This means that vesicles should consist of excreted cell plasma compartments, underlining that the AuNPs are not accumulating within the cell's nuclei. Moreover, the vesicles within in the cells showed a higher fluorescence signal for both membrane Orange and NIR dye.

Radio-sensitizing Experiments

The developed AuNPs are useful for diagnosis but could also serve as therapeutic agents in form of radioactive [198Au]AuNPs or as radio-sensitizer for X-ray irradiation. In this work, their ability as radio-sensitizer was evaluated by irradiation of AuNP-incubated DNA and subsequent gel electrophoresis. AuNPs are effective secondary electron emit- ters when irradiated with X-rays due to their high photoelectric absorption and their application as radio-sensitizers in nuclear medicine is lively discussed. If they are exaggerated by an external radiation source, Auger-Meitner electrons (AMEs) are emitted. This property was tested at the most prominent cell damage: double strand breaks (DSBs) of DNA.

The induced radiation damage to pUC19 plasmid DNA was investigated as a functions of dose and concentration of AuNPs. Indirectly induced single strand breaks (SSBs) were confirmed by using DMSO. DMSO can capture OH-radicals to form methanesulfinic acid (MSA) and is therefore a very prominent radical scavenger. The concentration of DMSO is high enough to reach a scavenging effect for several weeks. Two different AuNP derivatives, non-targeted AuNP-PEG 1 and targeted AuNP- RGD 7, were tested for their radio-sensitizing properties. The pUC19 plasmid DNA (280 kDa, 10 ng/µL per sample, BioLabs, New England) served as a

biological model. A semi- quantitative analysis was performed to prove the therapeutic efficiency of the AuNPs. To distinguish between DNA damage caused directly (e.g., by AE) and indirectly (especially by OH-radicals), all experiments were repeated in the presence of DMSO (2 M, applied as radical scavenger). DNA damage was quantified by agarose gel electrophoresis and com- pared with 1 Kb Plus DNA ladder protein (Thermo Fisher) and linear plasmid derived from pUC19 by BamH1-kit. Three different conformation states were evaluated: Super-coiled (native form, sc), open circular (according to SSBs, oc), and linear (after DSBs, lin) (Figure 12). After irradiation, 10 μL samples were mixed with 1.25 μL 10 × BlueJuice gel loading buffer for tracking of DNA migration. After gel electrophoresis (2 h at 120 V, 400 mA, 120 W) the gels were stained with ethidium bromide and the relative fluorescence intensities of the fractions were calculated (BioRad Fluorescence Analyzer) (Figures 12 and 13).
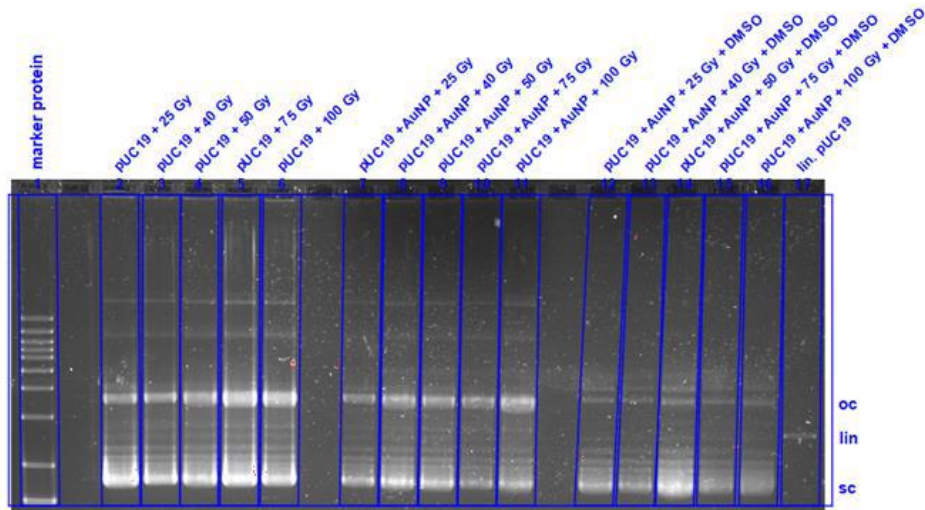

Figure no 13: Evaluation of the irradiation experiments using X-ray in combination with AuNP 1 via gel electrophoresis. Left line is the marker protein. The lowest bands show intact sc-DNA, middle bands show lin-DNA with DSBs, and the highest band show oc-DNA with SSBs. The direction of elution is from top to bottom

Figure no 14: Evaluation of the irradiation experiments using Re-188 in combination with AuNPs 1 via gel electrophoresis. Left line is the marker protein. The lowest bands show intact sc-DNA, middle bands show lin-DNA with DSBs, and the highest band show oc-DNA with SSBs. The direction of elution is from top to bottom
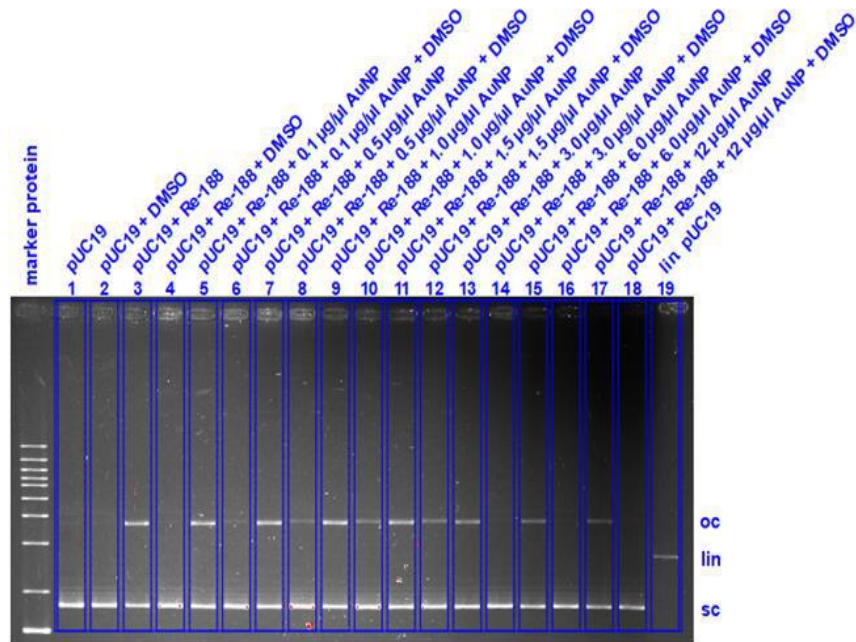
In Figure 15, SSBs without AuNPs are found in form of oc-DNA of 17–40% between 25–100 Gy X-ray irradiation (Maxishot Y.TU, Yxlon). DNA incubated with AuNP 1 (1.5 µg/µL) showed oc-DNA of 31–46% between 25–100 Gy X-ray irradiation, indicating a 14% higher SSB induction at a dose of 25 Gy and 6% more SSBs at a dose of 100 Gy. At lower doses, the higher radio-sensitizing effect of AuNP 1 was partially quenchable with DMSO to <10% oc-DNA. The radio-sensitizing effect was highest at 25 Gy. DSBs were induced in every experiment to the same extent ($3 \pm 2\%$) and were not quenchable by DMSO. There- fore, no direct DNA damage was observable, but a higher indirect DNA damage at AuNP- incubated DNA was found.
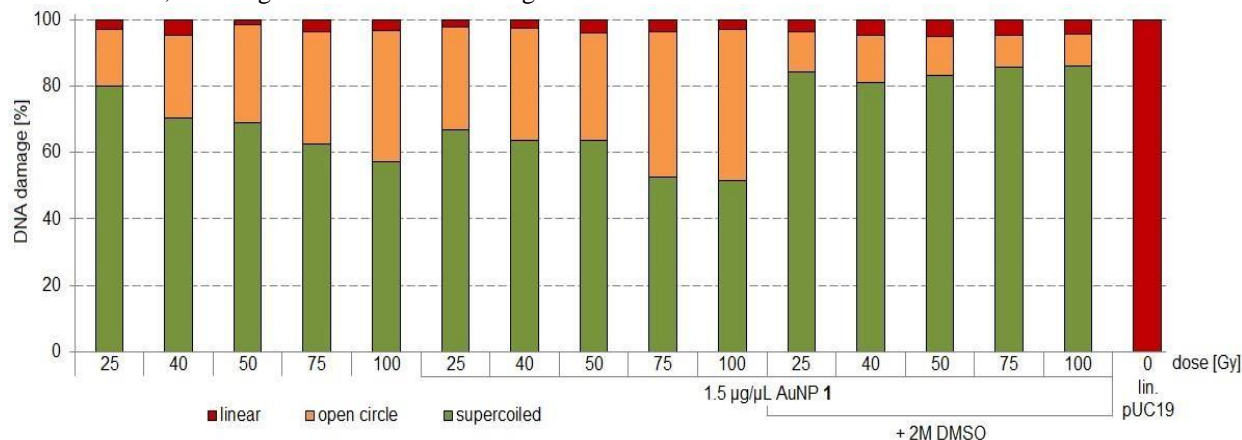

Figure no 15: Irradiation experiments applying different doses of 25, 40, 50, 75, and 100 GyforpUC19 only, pUC19 with AuNPs 1, and pUC19 with AuNPs1 inpresence of 2MDMSO. scpUC19 is expressed as green bar ,theexten to focis expressed in orange, and theexten to flin plas midinred

Next, the radiosensitizing effect at the same dose but different AuNP concentrations was evaluated (Figure 4). Further, we wanted to test whether it is possible to induce more DSBs by more production of AMEs, when the radiation source is in the direct vicinity of the AuNPs. For this experiment, Re-188-solution as inducer for radiosensitizing effects was chosen with its characteristic 2.12 MeV β- emission and 155 keV γ-coemission.
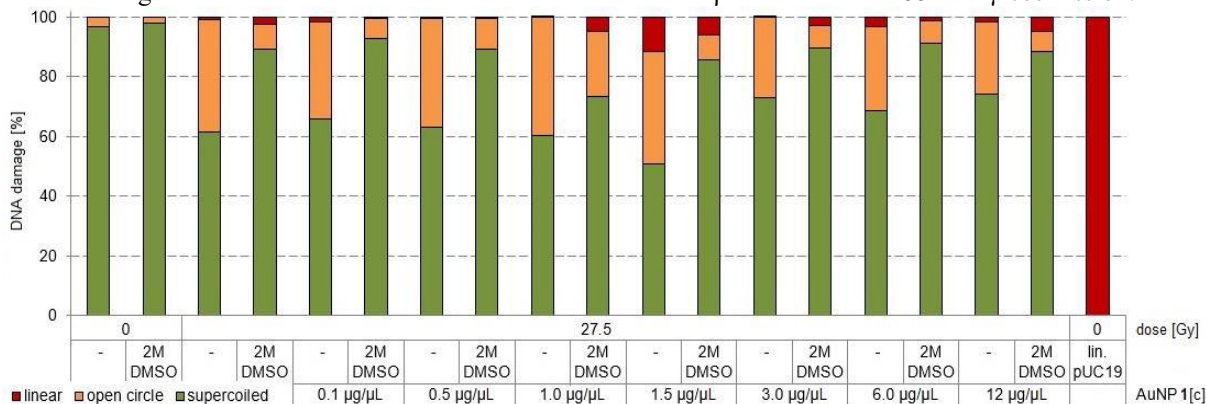

Figure no 16: Irradiation experiments with 27.5 Gy Re-188 at different concentrations of AuNP-PEG 1 for pUC19 only, pUC19 with AuNPs and pUC19 with AuNPs in combination with DMSO. sc pUC19 is expressed as green bar, the extend of oc is expressed in orange and the extend of lin plasmid in red

The highest effect for radiosensitizing was determined for 27.5 Gy as incubation dose. To reach this dose, 0.5 MBq Re-188 within 18 h incubation time in a 50 µL volume in a 1.5 mL Ep- pendorf vial were calculated using Formula 1. AuNP concentrations from 0.1–12.0 µg/µL were tested. Interestingly, an optimal radiosensitizing effect for AuNP-concentrations be- tween 1.0–1.5 µg/µL was found. At these AuNP-concentrations the direct DNA damage in form of DSBs was 4.8–11.7%. This effect was completely quenchable by 2 M DMSO for Re-188 alone, meaning that there are only nascenting OH-radicals responsible for the DNA damage. In contrast, by the combination of Re-188 with AuNPs 1, this effect was only partially quenchable by 2 M DMSO, meaning that additional AMEs from the AuNPs have a direct impact to the DNA damage (Figure 17).
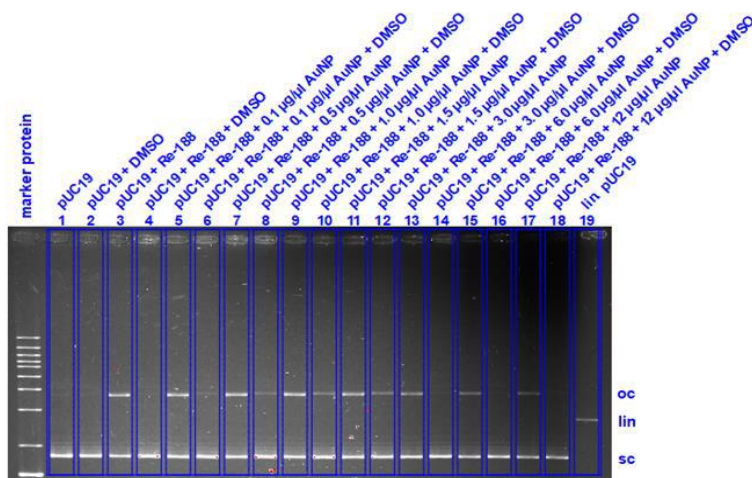
Figure no 17: Evaluation of the irradiation experiments using Re-188 in combination with AuNPs 1 via gel electrophoresis. Left line is the marker protein. The lowest bands show intact sc-DNA, middle bands show lin-DNA with DSBs, and the highest band show oc-DNA with SSBs. The direction of elution is from top to bottom

From these experiments it can be concluded that Re-188 in combination with AuNPshave a higher radiosensitizing effect than X-rays in combination with AuNPs. This effect has to be studied further. Formula (1) Calculation of ground dose in a 6-well-plate or Eppendorf vial for Re-188 by Geant4-simulation. D: energy dose, S: S-value, A: activity, T1/2: half-live of radionuclide, T: irradiation time.

Colony Formation Assay (CFA)

The radio-sensitizing effect found for the DNA experiments was repeated in vitro by irradiation of AuNP-incubated and non-incubated A431 cells and subsequent CFA. AuNPs within cell plasma are discussed to damage certain plasma compartments by additionally produced Auger-Meitner-electrons during X-ray irradiation. This hypothesis was proven in a pilot experiment. First, AuNPs 1 were tested for cell toxicity with different concentrations on A431 cells by CFA. No cell toxicity was found up to a concentration of 1 mg/mL (2.9 μM) (Figure 18) comparable with the literature data. Therefore, A431 cells were incubated with and without AuNPs 1 and 7 24 h before irradiation. After incubation, the cells were washed and subsequently treated with doses of 0– 10 Gy by X-ray irradiation. Afterwards, the cells were seeded for CFA. Indeed, a low difference in survival fractions for AuNP-incubated and a non-incubated cell was found for a dose of 2 Gy (Figure 19. A slightly lower survival fraction for AuNP-incubated cells was found at 4 Gy for AuNP-RGD 7 $(8.0 \pm 1.5)\%$ but not for AuNP-PEG 1 $(15.0 \pm 2.6)\%$ com- pared to cells in absence of AuNPs $(14.9 \pm 2.1)\%$. A clearly much lower survival fraction at a dose of 6 Gy was found for AuNPs 7 $(1.9 \pm 0.7)\%$ and AuNP 1 $(2.9 \pm 0.7)\%$ compared to cells in absence of AuNPs $(7.2 \pm 0.8)\%$ (Figures 5 and A22), indicating a radio-sensitizing effect.
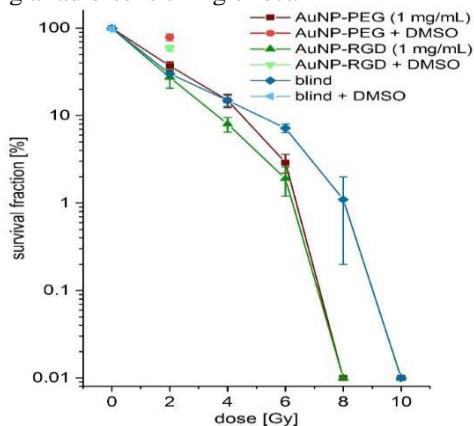

Figure no 18: Survival fractions in logarithmic scale of the colony formation assays at different X-ray doses (0–10 Gy) with AuNPs 1 (red), AuNPs 7 (green), and without AuNPs (blue) incubation. Single colony formation assays (CFAs) with DMSO are shown at 2 Gy for AuNPs 1 (light red) and AuNPs 7 (light green) and at 0 Gy in absence of AuNP (light blue)
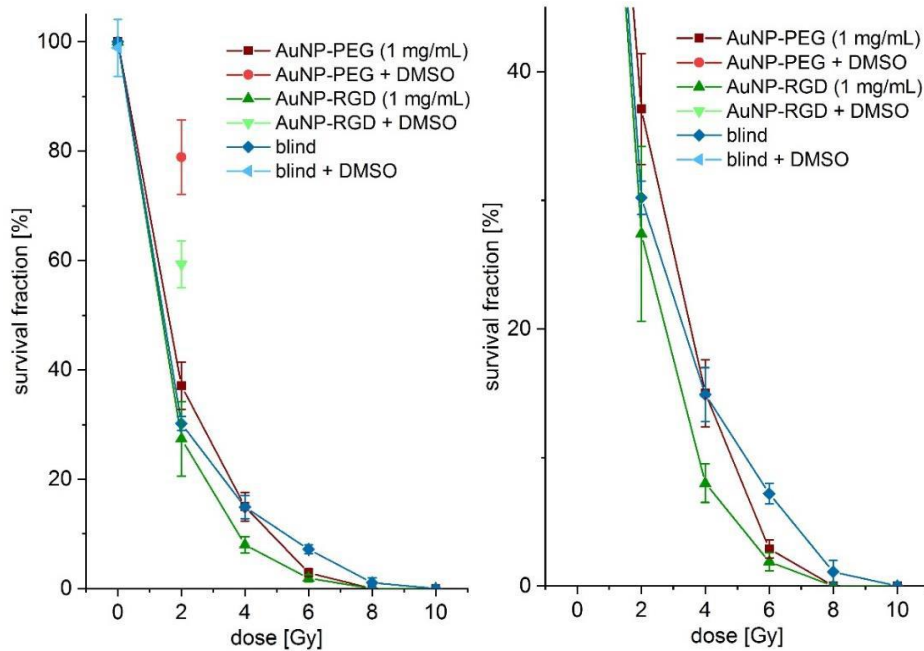
Figure no 19: Colony formation assay with survival fraction 0–105% linear (left) and zoom 0–45% linear (right)

Further, at a dose of 8 Gy, no colony formation was found for AuNP-incubated cells. Furthermore, at a dose of 10 Gy, no colony formation was found for cells in absence of AuNPs. Interestingly, the specific AuNPs 7 showed a stronger effect at a dose of 4 and 6 Gy compared to non-specific AuNPs 1. At a dose of 2 Gy, the cells were also incubated with 0.2 M DMSO as radical scavenger during irradiation. The factor 10 less DMSO concentration is important for cell life. These fractions showed lower cell damage for AuNP 7 (59.3 ± 4.3)% and much lower cell damage for AuNP 1 (78.9 ± 6.8). Non-incubated cells showed cell survival of (98.9 ± 5.2)% with 0.2 M DMSO at a dose of 0 Gy, indicating no toxic effects at these conditions.
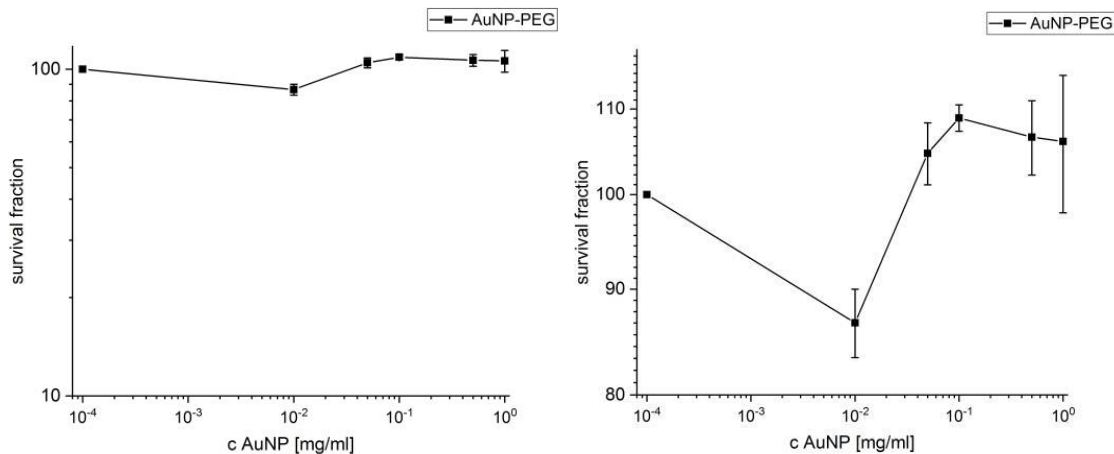

Figure no 20: Toxicology assay for AuNP-PEG 1 with survival fraction 10–100% logarithmic scale (left) and 80–110% linear scale (right)

In Vivo Experiments

In order to prove the concept of receptor-specific tumor accumulation of the peptide- functionalized particles and their suitability for optical imaging in vivo, two A431-tumor bearing mice were injected with AuNPs 8 according to previously established protocols [43]. In brief, the mice were injected with 75 µg AuNPs 8 in 100 µL sterile PBS. The injected amount of AuNPs 8 corresponded to 1.5 µg (1.75 nmol) of NIR-dye per animal as AuNPs 8 contain 2% dye (see Table 1). This amount is comparable to literature values of 1–50 µg/g for cyanine-dye conjugates for in vivo fluorescence imaging of tumors [10,49,60–62]. The mice were measured repeatedly over a period of up to 72 h post injection (p.i.) with a fluorescence imager (In Vivo Xtreme, Bruker) (Figure 21) by using 730 nm as excitation wavelength and 790 nm as emission wavelength.

A very low background signal was found, which is assumed to derive from the chlorophyll-containing diet of the mice. After injection of AuNPs 8, the background signal faded to the underground and a fast renal clearance of an excess of AuNPs 8 was observed in vivo. AuNPs 8 were found ex vivo in the collected urine and showed no degradation when analyzed by HPLC. The tumor-to- muscle ratio increased during the time of observation. The accumulation was measured by region-of-interest (ROI) interpretation (Figure 22), and after 72 h, an ex vivo biodis- tribution (Figure 23) was performed and compared with the obtained in vivo data. The accumulation values detected by in vivo measurements and biodistribution experiments were found to be comparable for tumor, muscle, and kidney but different for the liver, since in biodistribution experiments, the weight of the organs was also considered and the organs could be measured directly (Figure 24, Table 2), whereas in live imaging, the signal of the liver was found to be relatively lower, since the organ was measured from the back of the mice. However, the animal experiments revealed a higher accumulation of AuNPs 8 in the A431-tumor in comparison to muscle at 3–72 h post i.v. injection.

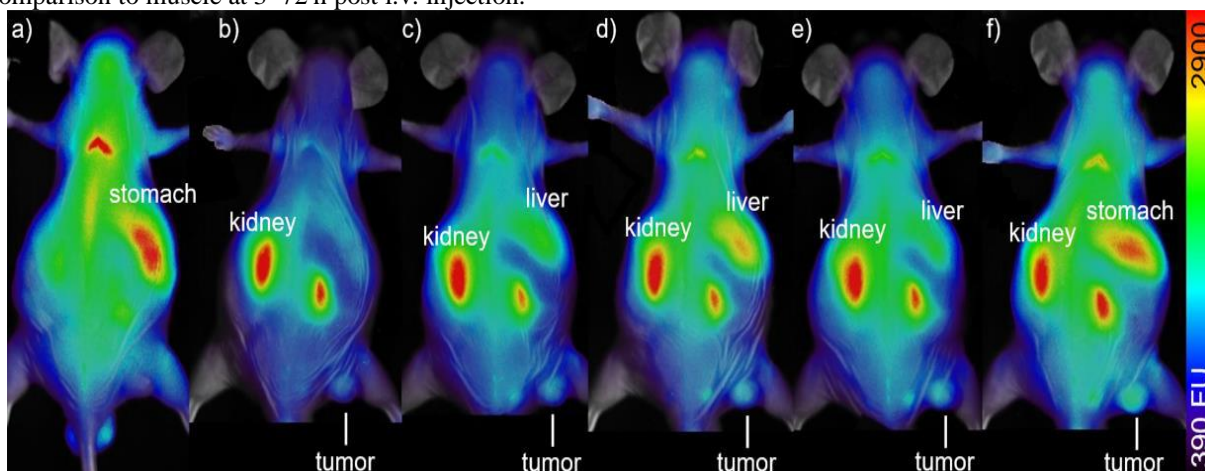**Figure no 21:** In vivo biodistribution of 50 µg/100 µL AuNPs 8 in a A431-tumorbearing mouse: (a) fluorescence before injection, (b) 4 h p.i., (c) 21 h p.i., (d) 28 h p.i., (e) 48 h p.i., and (f) 72 h p.i. Ratio tumor: muscle: liver: kidney/g = 4.4:1.0:0.6:5.4 (e)
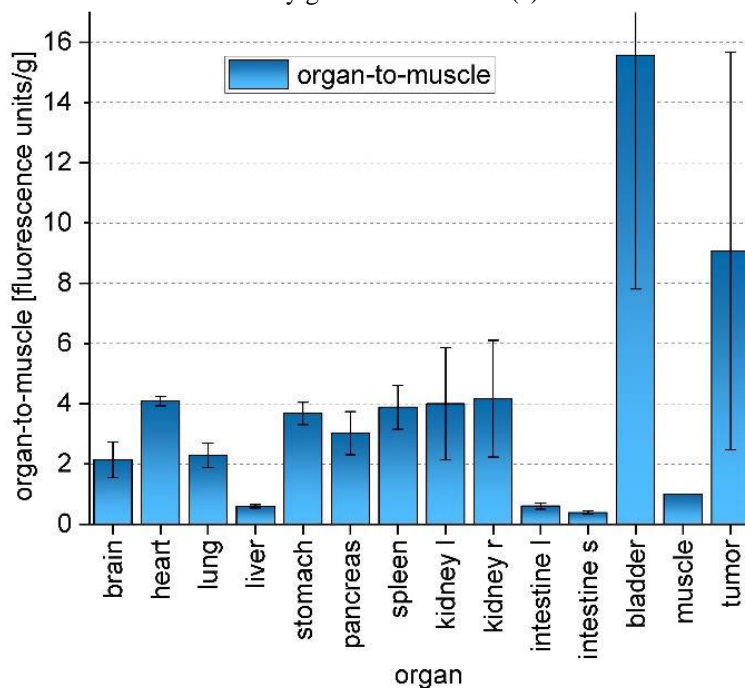

Figure no 22: Biodistribution of AuNPs 8 at 72 h p.i. Values are given in measured fluorescence units per organ weight (n = 2)
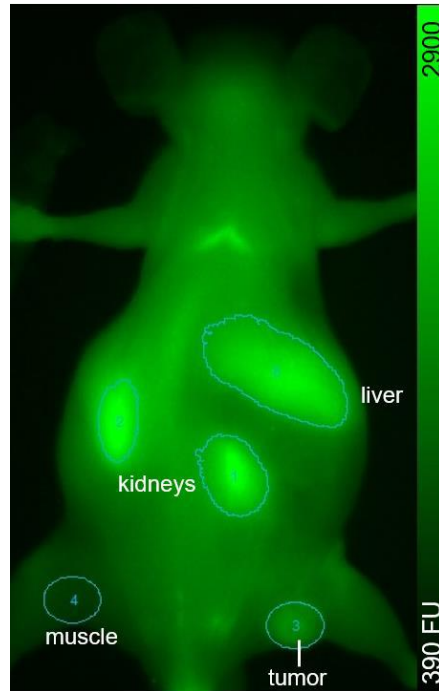
Figure no 23: Regions of interest (ROIs) of organs during live imaging in vivo 48 h p.i. as examplefor AuNP-RGD-NIR-dye 8: ratio-to-muscle of kidneys 2.40 ± 0.12, tumor 1.47 ± 0.07, and liver 2.20 ± 0.11
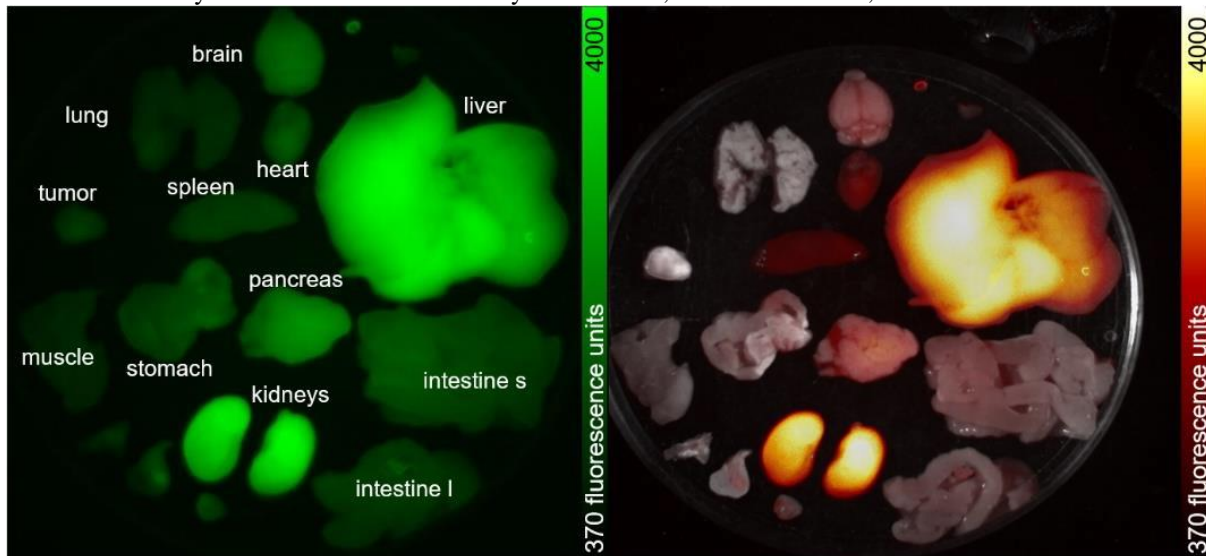
Figure no 24: Ex vivo biodistribution of AuNP-RGD-NIR-dye 8 at A431-tumor-bearing mouse
Table no A1: Biodistribution of AuNP-RGD-NIR-dye 8 in A431 tumor-bearing mice.
MFU = Mean fluore scence units

Organ	Weight (gm)	MFU/g	Ratio-to-Muscle/g
Pancreas	0.387	5089	3.53
Kidney Left	0.383	7651	5.31
Kidney Right	0.383	7975	5.31
Heart	0.226	5730	3.98
Lung	0.236	3709	2.58
Muscle	0.558	1440	1.00
Brain	0.417	3690	2.56
Intestine large	1.096	983	0.68
Spleen	0.228	4857	3.37
Stomach	0.252	4923	3.42

Intestine small	2.537	499	0.35
Liver	3.215	927	0.64
Gall bladder	0.034	30329	21.06
Tumor	0.148	6346	4.41

IV. Discussion

Stable αvβ3-specific AuNPs 7 were successfully synthesized with a slightly better avidity compared to the monomeric peptide ligand c(RGDfK). AuNPs additionally deco- rated with an NIR-dye had a slightly lower avidity as compared with the monomeric RGD-ligand, since in this case, a lower number of RGD ligands is located on the surface of the AuNPs (Table A1). Via confocal fluorescence microscopy, the fate of AuNPs 8 on A431 cells was observed within 1–24 h. The AuNPs started to concentrate within the cell plasma but not within the nuclei as confirmed by confocal microscopy. Additionally, the formation of vesicles after 24 h and their excretion could be verified.

The fluorescence signal started to concentrate in small dots within the cell plasma and in the extracellular medium those small foci could be observed too, indicating the excretion of the AuNPs in form of vesicles. This vesicle formation and excretion from cells within 24 h after incubation is perhaps a certain property of the AuNPs, when healthy tissue should expel therapeutic AuNPs. Within tumor tissue, the vesicles may stick in the interstitial cell region because of the lower blood supply and lower nutrition exchange with the surrounding tissues, presup- posed that the AuNP would penetrate the deep tumor tissue. The activation of AuNPs by X-rays to emit AMEs was tested at pUC19 DNA incubated with AuNPs 1. No additional DSBs were found for all doses (25–100 Gy). Interestingly, additional SSBs (14%) in the presence of AuNP 1 were found at 25 Gy com- pared to non-AuNP-incubated DNA.

Those SSBs were not inhabitable by DMSO, indicating the emission of AMEs from the AuNPs by external X-ray irradiation due to direct DNA damage without influence of OH-radicals. It is known that AuNPs can degrade DNA to little extend (1–2%) but does not increase significantly for longer time (weeks) and with organic solvents or no-neutral pH. To further investigate this phenomenon, an experiment with AuNP 1 and 7 at concentrations of 1 and 10 μg/mL was per- formed to evaluate the impact of the AuNPs to the degradation of DNA (Figure 25 and 26).

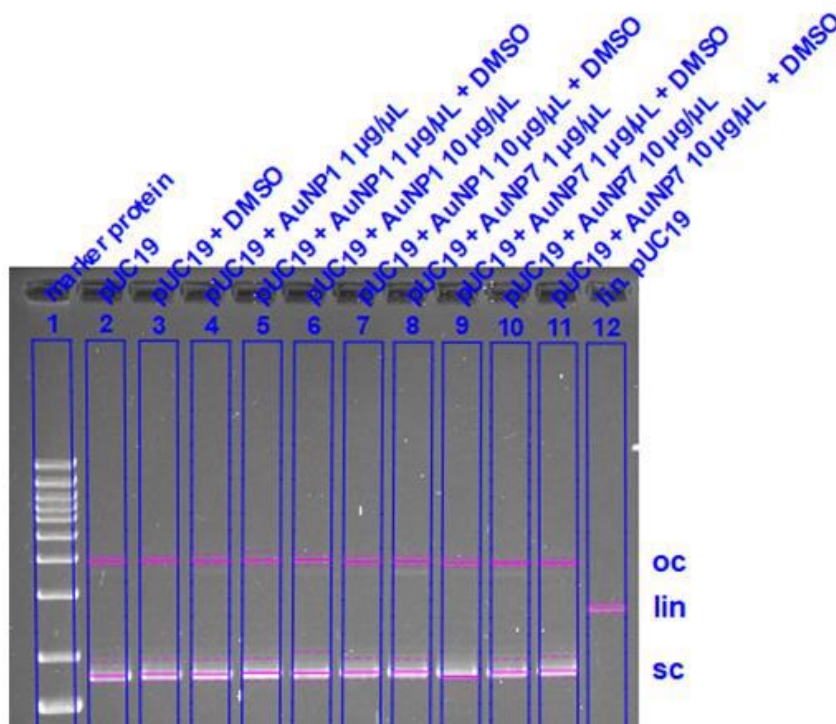**Figure no 25:** Evaluation of influence to DNA degradation of AuNP 1 and 7 at a concentration of 1and 10 μg/mL with and without 2 M DMSO via gel electrophoresis. Left line is the marker protein. The lowest bands show intact sc-DNA, middle bands show lin-DNA with DSBs, and the highest band show oc-DNA with SSBs. The direction of elution is from top to bottom
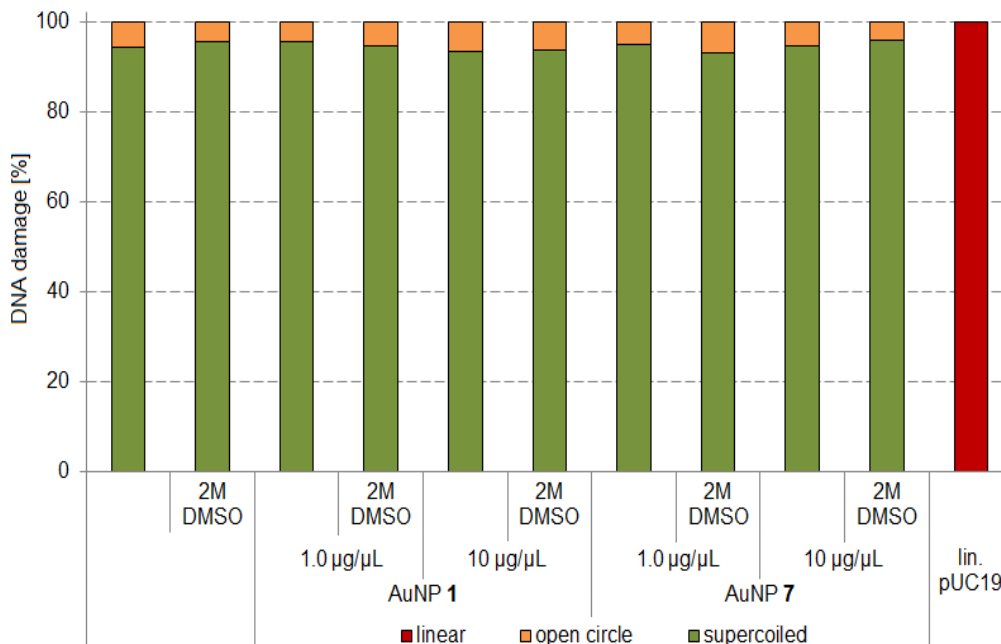
Figure no 26: Influence of AuNPs 1 and 7 to the degradation of pUC19 DNA applying different concentrations of 0, 1, and 10 μg/μL with and without 2 M DMSO. sc pUC19 is expressed as green bar, the extent of oc is expressed in orange, and the extent of lin plasmid in red

The DNA degradation was not significantly different for all experimental conditions, and the formation of oc-DNA was at (5.48 ± 0.95)%. As for our experimental setting (2 h incubation, neutral pH), we can exclude that the >10% DNA damage is from the AuNP itself, but most prominent due to the induction of AMEs [65]. Further, an optimum for the AuNP concentration between 0.5–1.5 mg/mL was determined by incubation of DNA with Re-188 solution. The reason for this observation may be guessed by taking into account that at lower AuNP concentrations the number of additionally produced AMEs are too low for a visible DNA damage, whereas at higher concentrations, the AuNPs could shield the AMEs from a neighboring AuNP and Re-188. With DMSO as radical scavenger, the DNA damage was not completely quenchable.

The Auger–Meitner effect has a very short effective range of ~2 nm3 in vivo and is most effective when directly incorporated into the DNA. Therefore, a nanoparticle not exceeding a diameter of 5 nm could in theory be an effective Auger-emitter in a volume of ~9 nm3 when activated with X-rays. This is a very short range within a cell, which has a typical diameter of 120–200 μm. In vitro fluorescence microscopy confirmed (Figure A16) the accumulation of AuNPs in the cell plasma but not in the nuclei. For this reason, direct DNA damage can be excluded. Due to their behavior, the AuNPs could reach other cell compartments in the cell plasma that are also important for cell life. Auger–Meitner electrons could then damage those compartments and the cell is about to die. This hypothesis was evaluated in the following experiment: First, we carried out in vitro radio-sensitizing experiments with AuNP-PEG 1 and AuNP-RGD 7 on A431 cells showing a similar effect as compared with literature data. In the CFA experiments (Figure 5), AuNPs 1 and 7 did not have a much higher effect at a dose of 2 Gy compared to reference experiments in absence of AuNPs and had a slightly higher effect at 4 Gy compared to the untreated cells. AuNPs 7 had a higher effect at 6 Gy compared to AuNPs1.

These findings could be explained by a faster accumulation of the targeted AuNPs 7 from the medium into the cell plasma compared to unspecific AuNPs 1 and other AuNP-species. Perhaps bigger AuNPs could produce more Auger electrons or remain within the cells for a longer period of time, thereby allowing a higher effect to be observed. In addition, bigger gold nanorods (AuNRs) functionalized with RGD peptides could be an interesting Auger–Meitner emitter. Initial in vivo experiments with AuNP-RGD-NIR-dye 8 showed a similar tumor ac-cumulation and bio-distribution within 72 h as compared to other NIR-dye-functionalized AuNPs. In fluorescence live-imaging the organ-to-muscle ratios were 2.40 ± 0.12 (kid- neys), 1.47 ± 0.07 (tumor), and 2.20 ± 0.11 (liver) (Figure A7). In bio-distribution experiments, a significantly higher uptake in the tumor was found compared to the muscles (Figure 7). There was a relatively large difference in tumor uptake due to the different growth rate of the tumors. It is known that growing tumors have a high angiogenesis level and therefore a higher αvβ3-integrine expression. Hence, a higher uptake of RGD-functionalized AuNPs in a fast-growing tumor is explainable.

V. Conclusion

These initial results prove that the dually modified particles show potential as imaging tools for αvβ3-expressing tumors in vivo via optical imaging. Especially for long-term observations of in vivo processes, the AuNPs could be useful. Since their accumulation is from slower nature (>1 d), the AuNPs cannot be used for short-term investigations such as Ga-68-PET. Further, the AuNPs could also serve as a tool for characterization of cell cycles and behavior by confocal fluorescence microscopy or live-cell microscopy. Interestingly, different modifications lead to different cell answer such as vesiculation and excretion. In vitro experiments for the assessment of the radio-sensitizing ability of the AuNPs showed limited effects for the ultra-small AuNPs. However, in vivo, a major amount of AuNPs is excreted very fast renally. The rest of AuNPs accumulate in target organs and have a high retention there. Therefore, these AuNPs could serve as tool for radiotherapy as radio-sensitizer or as activated [198Au]AuNPs. Further in vivo experiments for the determination of radio-sensitizing effects for bigger AuNPs and AuNRs and also for [198Au]AuNPs are underway.

References

[1].   Mayo, R.L.; Robinson, F.R.S. Auger and secondary X-ray electrons from gold. Royal Soc. Pub. 1939, 173, 192–200.

[2].   Zhang, X.D.; Wu, D.; Shen, X.; Chen, J.; Sun, Y.M.; Liu, P.X.; Liang, X.J. Size-dependent radiosensitization of PEG-coated goldnanoparticles for cancer radiation therapy. Biomaterials 2012, 33, 6408–6419, doi:10.1016/j.biomaterials.2012.05.047.

[3].   Hainfeld, J.F.; Slatkin, D.N.; Smilowitz, H.M. The use of gold nanoparticles to enhance radiotherapy in mice. Phys. Med. Biol.2004, 49, N309–N315, doi:10.1088/0031-9155/49/18/n03.

[4].   Säterborg, N.E. The distribution of 198Au injected intravenously as a colloid and in solution. ActaRadiol. Ther. Phys. Biol. 1973,12, 509–528.

[5].   Khan, M.K.; Minc, L.D.; Nigavekar, S.S.; Kariapper, M.S.T.; Nair, B.M.; Schipper, M.; Cook, A.C.; Lesniak, W.G.; Balogh, L.P.Fabrication of {198Au0} radioactive composite nanodevices and their use for nano-brachytherapy. Nanomed.Nanotechnol. Biol.Med. 2008, 4, 57–69.

[6].   Chakravarty, R.; Chakraborty, S.; Guleria, A.; Kumar, C.; Kunwar, A.; Nair, K.V.V.; Sarma, H.D.; Dash, A. Clinical scalesynthesis of intrinsically radiolabeled and cyclic RGD peptide functionalized 198Au nanoparticles for targeted cancer therapy.Nucl. Med. Biol. 2019, 72–73, 1–10, doi:10.1016/j.nucmedbio.2019.05.005.

[7].   Makrigiorgos, G.; Adelstein, S.J.; Kassis, A.I. Auger electron emitters: Insights gained from in vitro experiments. Radiat. Environ.Biophys. 1990, 29, 75–91.

[8].   Hauck, T.S.; Ghazani, A.A.; Chan, W.C. Assessing the effect of surface chemistry on gold nanorod uptake, toxicity, and geneexpression in mammalian cells. Small 2008, 4, 153–159, doi:10.1002/smll.200700217.

[9].   Pan, Y.; Neuss, S.; Leifert, A.; Fischler, M.; Wen, F.; Simon, U.; Schmid, G.; Brandau, W.; Jahnen-Dechent, W. Size-dependentcytotoxicity of gold nanoparticles. Small 2007, 3, 1941–1949, doi:10.1002/smll.200700378.

[10]. Mironava, T.; Hadjiargyrou, M.; Simon, M.; Jurukovski, V.; Rafailovich, M.H. Gold nanoparticles cellular toxicity and recovery:Effect of size, concentration and exposure time. Nanotoxicology 2010, 4, 120–137, doi:10.3109/17435390903471463.

[11]. Cai, Q.Y.; Yu, P.; Besch-Williford, C.; Smith, C.J.; Sieckman, G.L.; Hoffman, T.J.; Ma, L. Near-infrared fluorescence imaging ofgastrin releasing peptide receptor targeting in prostate cancer lymph node metastases. Prostate 2013, 73, 842–854, doi:10.1002/pros.22630.

[12]. Chen, H.; Wan, S.; Zhu, F.; Wang, C.; Cui, S.; Du, C.; Ma, Y.; Gu, Y. A fast tumor-targeting near-infrared fluorescent probe basedon bombesin analog for in vivo tumor imaging. Contrast Media Mol. Imaging 2014, 9, 122–134, doi:10.1002/cmmi.1545.

[13]. Ma, L.; Yu, P.; Veerendra, B.; Rold, T.L.; Retzloff, L.; Prasanphanich, A.; Sieckman, G.; Hoffman, T.J.; Volkert, W.A.; Smith, C.J.In vitro and in vivo evaluation of alexafluor 680-bombesin[7–14]NH2 peptide conjugate, a high-affinity fluorescent probe withhigh selectivity for the gastrinreleasing peptide receptor. Mol. Imaging 2005, 16, 171–180.

[14]. Herdt, A.R.; Drawz, S.M.; Kang, Y.; Taton, T.A. DNA dissociation and degradation at gold nanoparticle surfaces. Colloids Surf.,B 2006, 51, 130–139, doi:10.1016/j.colsurfb.2006.06.006.

[15]. Bhatt, N.; Huang, P.J.; Dave, N.; Liu, J. Dissociation and degradation of thiol-modified DNA on gold nanoparticles in aqueousand organic solvents. Langmuir ACS J. Surf. Colloids 2011, 27, 6132–6137, doi:10.1021/la200241d.

[16]. Igaz, N.; Szoke, K.; Kovacs, D.; Buhala, A.; Varga, Z.; Belteky, P.; Razga, Z.; Tiszlavicz, L.; Vizler, C.; Hideghety, K.; et al.Synergistic radiosensitization by gold nanoparticles and the histone deacetylase inhibitor SAHA in 2D and 3D cancer cellcultures. Nanomaterials 2020, 10, doi:10.3390/nano10010158.

[17]. Kassis, A.I. Molecular and cellular radiobiological effects of Auger emitting radionuclides. Radiat. Prot. Dosim. 2011, 143, 241–247, doi:10.1093/rpd/ncq385.

[18]. Chanda, N.; Kan, P.; Watkinson, L.D.; Shukla, R.; Zambre, A.; Carmack, T.L.; Engelbrecht, H.; Lever, J.R.; Katti, K.; Fent, G.M.;et al. Radioactive gold nanoparticles in cancer therapy: Therapeutic efficacy studies of GA-198AuNP nanoconstruct in prostatetumor-bearing mice. Nanomedicine : nanotechnology, biology, and medicine 2010, 6, 201–209, doi:10.1016/j.nano.2009.11.001.

[19]. Pretze, M.; Hien, A.; Roscher, M.; Richter, K.; Rädle, M.; Wängler, C.; Wängler, B. Efficient modification of GRPR-specific goldnanoparticles for fluorescence imaging of prostate carcinoma. J. Labelled Compd. Radiopharm. 2017, 60, S601, doi:10.1002/jlcr.3508.

[20]. Hien, A.; Pretze, M.; Braun, F.; Schäfer, E.; Kümmel, T.; Roscher, M.; Schock-Kusch, D.; Waldeck, J.; Müller, B.; Wängler, C.; etal. Non-contact recognition of fluorescently labeled objects in deep tissue via optimized optical arrangement. PLoS ONE 2018,13, e0208236, doi:10.1371/journal.pone.0208236.

[21]. Zhu, J.; Chin, J.; Wängler, C.; Wängler, B.; Lennox, R.B.; Schirrmacher, R. Rapid 18F-labeling and loading of PEGylated goldnanoparticles for in vivo applications. Bioconjug. Chem. 2014, 25, 1143–1150, doi:10.1021/bc5001593.

[22]. Zhao, Y.; Sultan, D.; Detering, L.; Cho, S.; Sun, G.; Pierce, R.; Wooley, K.L.; Liu, Y. Copper-64-alloyed gold nanoparticles forcancer imaging: improved radiolabel stability and diagnostic accuracy. Angew. Chem. Int. Ed. 2014, 53, 156–159,doi:10.1002/anie.201308494.

[23].   Pretze, M.; van der Meulen, N.P.; Wängler, C.; Schibli, R.; Wängler, B. Targeted 64Cu-labeled gold nanoparticles for dual imagingwith positron emission tomography and optical imaging. J. Labelled Comp. Radiopharm. 2019, 62, 471–482, doi:10.1002/jlcr.3736.

[24].   Jiménez-Mancilla, N.; Ferro-Flores, G.; Santos-Cuevas, C.; Ocampo-García, B.; Luna-Gutiérrez, M.; Azorín-Vega, E.; Isaac-Olivé,K.; Camacho-López, M.; Torres-García, E. Multifunctional targeted therapy system based on 99mTc/177Lu-labeled goldnanoparticles-Tat(49-57)-Lys3-bombesin internalized in nuclei of prostate cancer cells. J. Labelled Compd. Radiopharm. 2013, 56,663–671, doi:10.1002/jlcr.3087.

[25].   Kim, M.S.; Lee, E.J.; Kim, J.W.; Chung, U.S.; Koh, W.G.; Keum, K.C.; Koom, W.S. Gold nanoparticles enhance anti-tumor effectof radiotherapy to hypoxic tumor. Radiat. Oncol. J. 2016, 34, 230–238, doi:10.3857/roj.2016.01788.

[26].   Black, K.C.L.; Wang, Y.; Luehmann, H.P.; Cai, X.; Xing, W.; Pang, B.; Zhao, Y.; Cutler, C.S.; Wang, L.V.; Liu, Y.; et al. Radioactive198Au-Doped Nanostructures with Different Shapes for In Vivo Analyses of Their Biodistribution, Tumor Uptake, andIntratumoral Distribution. ACS Nano 2014, 8, 4385–4394, doi:10.1021/nn406258m.

[27].   Cui, S.; Yin, D.; Chen, Y.; Di, Y.; Chen, H.; Ma, Y.; Achilefu, S.; Gu, Y. In vivo targeted deep-tissue photodynamic therapy basedon near-infrared light triggered upconversionnanoconstruct. ACS Nano 2013, 7, 676–688, doi:10.1021/nn304872n.

[28].   Shukla, R.; Chanda, N.; Zambre, A.; Upendran, A.; Katti, K.; Kulkarni, R.R.; Nune, S.K.; Casteel, S.W.; Smith, C.J.; Vimal, J.; etal. Laminin receptor specific therapeutic gold nanoparticles (198AuNP-EGCg) show efficacy in treating prostate cancer. Proc.Natl. Acad. Sci. USA 2012, 109, 12426–12431, doi:10.1073/pnas.1121174109.

[29].   Maeda, H.; Fang, J.; Inutsuka, T.; Kitamoto, Y. Vascular permeability enhancement in solid tumor: various factors, mechanismsinvolved and its implications. Int. Immunopharmacol. 2003, 3, 319–328, doi:10.1016/s1567-5769(02)00271-0.

[30].   Zarschler, K.; Rocks, L.; Licciardello, N.; Boselli, L.; Polo, E.; Garcia, K.P.; De Cola, L.; Stephan, H.; Dawson, K.A. Ultrasmallinorganic nanoparticles: State-of-the-art and perspectives for biomedical applications. Nanomed.Nanotechnol. Biol. Med. 2016, 12,1663–1701, doi:10.1016/j.nano.2016.02.019.

[31].   Frens, G. Controlled Nucleation for the Regulation of the Particle Size in Monodisperse Gold Suspensions. Nat. Phys. Sci. 1973,241, 20–22, doi:10.1038/physci241020a0.

[32].   Brust, M.; Walker, M.; Bethell, D.; Schiffrin, D.J.; Whyman, R. Synthesis of Thiol-derivatised Gold Nanoparticles in a Two-phaseLiquid-Liquid System. J. Chem. Soc. Chem. Commun. 1994, 801–802, doi:10.1039/C39940000801.

[33].   Turkevich, J. Colloidal Gold. Part I—Historical and preparative aspects, morphology and structure. Gold Bull. 1985, 18, 86–91,doi:10.1007/BF03214690.